Journal of Microscopy, Vol. 181, Pt 1, January 1996, pp. 2–9.
Received 22 November 1994; accepted 1 August 1995

Polystyrene spheres on mica substrates: AFM calibration, tip parameters and scan artefacts

M. VAN CLEEF, S. A. HOLT, G. S. WATSON & S. MYHRA
Faculty of Science and Technology, Griffith University, Nathan, Queensland 4111, Australia

Key words. Force microscopy, polystyrene spheres, tip parameters, scan artefacts, noncontact mode.

Summary

Atomic force microscopy (AFM), in various versions, has had major impact as a surface structural and spectroscopic tool since its invention in 1986. At its present state of development, however, the interpretation of AFM images is limited by the current state of methodologies for calibration over the wide dynamic range of magnification. Also, the parameters of individual tips, as well as the generic characteristics of different kinds of tips, affect both the quality of the images and their interpretation. Finally, the very nature of the tip-to-surface interaction will generate artefacts, in addition to those associated with tip shape, which need to be fully understood by the practitioners of force microscopy. This project seeks to address and shed light on some of these issues.

Polystyrene beads deposited on mica substrates form hexagonal close-packed layers. The unit cell parameters are suitable for calibration of the AFM in the lateral plane, while the perpendicular spacing of the layers is appropriate for calibration along the vertical axis. Using different size fractions, it is straightforward to determine the extents of linearity, orthogonality, thermal and instrumental drifts over distances from 100 nm to tens of micrometres. The present results show that the methodologies for contact mode operation can be adapted to noncontact modes.

It is known that an AFM image arises from a convolution of surface topography and tip shape, and is mediated by the interaction. In principle it is possible to carry out a deconvolution, if we have complete knowledge about two of the three elements (i.e. tip, surface and interaction). In practice we rarely have the requisite information. Prominent artefacts will occur when the characteristic parameters of the tip are comparable to those of the surface topography, and/or if there is a variable strength, or extent of localization, of the interaction. The present results demonstrate artefacts due to effects of geometry as well as interaction.

Introduction

A generic scanned probe system consists of three essential elements: a sharp tip which must be locatable and controllable in space; a surface with particular topographic and structural properties; and a localized interaction between tip and surface having a strength which depends on the tip-to-surface separation, and which is responsive to topographic and/or structural changes. The most significant consequence of this description is that given complete information about any two of the three elements, there is the implication that, in principle, complete knowledge about the third must be obtainable.

The first member of the recent family of scanned probe microscopes (SPM) was the scanning tunnelling microscope (STM), invented by Binnig *et al.* (1982). This development was anticipated by the work of Young *et al.* (1972), who achieved three-dimensional imaging with the 'Topographiner'. The next member, the atomic force microscope (AFM), was demonstrated 4 years later by Binnig *et al.* (1986). Subsequently, other interactions (e.g. magnetostatic, electrostatic, thermal radiation, etc.) have generated additional members, ably described by Wickramasinghe (1990). As well, each of the original techniques has had offsprings by way of variations on the theme – such as contact, noncontact, lateral force and force constant spectroscopic modes for the AFM.

In many respects AFM is a technique at the steepest part of the learning curve. For instance, identification of image artefacts cannot be carried out on a routine basis, and establishing optimum imaging conditions remains very much an artform. Although these aspects have been the subjects of several recent studies (e.g. Wurster & Ocker, 1993; Odin *et al.*, 1994; Schwartz *et al.*, 1994; Xu & Arnsdorf, 1994), much work remains to be done in order to establish 'best practice' for AFM over the broad range of current and potential applications.

The present study seeks to exploit the ready availability of polystyrene spheres in the nanometre size range.

© 1996 The Royal Microscopical Society

Monodisperse spheres have been used as size calibration standards in optical and electron microscopy, and more recently for lateral and vertical calibration of AFM instruments operated in the contact mode (e.g. Li & Lindsay, 1991; Odin *et al.*, 1994). In the context of the generic description of an SPM system, however, it is relevant to note that the spheres may constitute a well-characterized surface. Accordingly it may be possible to shed additional light on the image formation process(es), and/or to probe the interaction forces between two bodies of known shapes and compositions.

The study had a number of objectives. The original intention was to extend the methodology of instrumental calibration to the noncontact mode. Secondly, during the course of the project there was a change of emphasis towards investigation of artefacts associated with the convolution of tip shape and surface topography, as well as with 'ghosts' arising from force 'delocalization' (we shall use 'delocalization' in a nonstandard sense, as a matter of convenience: see below for a full definition).

Experimental details

Polystyrene spheres and layer deposition

The polystyrene spheres (also known as Nanospheres™) were obtained from Duke Scientific Corporation. The relevant characteristics are listed in Table 1. The as-delivered batch was intended as a size standard for microscopy calibration and was supplied with certification from the manufacturer.

The as-received suspension was diluted with distilled and deionized water (DDW) to concentrations in the range 0·1–0·01% by volume. Following dilution the suspensions were dispersed by mechanical or ultrasonic agitation. Freshly cleaved mica surfaces (1-cm^2 areas) were used as substrates. A micropipette was used to deposit 5–50 μL of suspension on the substrate. The surface was then allowed to dry in air for a few minutes before being placed in a desiccator for a minimum of 8 h. The condition of the specimen surface was then examined with optical microscopy, in order to locate promising areas, and then subjected to AFM scanning.

Table 1. Specifications for Nanosphere™ size standards.

Parameter		200-nm batch
Mean diameter		198 ± 5 nm
Standard deviation		2·5 nm
Coefficient of variation		1·3%
Bead density		$4{\cdot}7 \times 10^{12}$ mL^{-1}
Suspension composition	Beads	2%
(by volume)	Water	92·9–98%
	Dispersant	0·2–5%
	Preservative	$< 0{\cdot}1$%
Composition		Polystyrene
Specific gravity		1·05 g/mL

AFM instrumentation and methods

A Topometrix TMX-2000 system was used throughout these investigations; the original contact mode instrument was fitted with a noncontact conversion kit. One of several stages (1, 10 and 70 μm) was used depending on requirements for field of view and spatial resolution. The imaging in the repulsive force regime was carried out in the constant force mode using a standard V-shaped cantilever with integral Si_3N_4 pyramidally shaped tip with a stated aspect ratio of 0·7 (height divided by base edge) and a radius of curvature of 40 nm. The nominal force constant was 0·032 N/m. The force constants of several levers from the same batch were estimated from direct measurements of dimensions and the resonant frequencies, and were found to be consistent with the stated value.

Imaging in the attractive force regime used an Si 'diving board' type of lever, again with an integral tip with a stated aspect ratio of 3:1 and radius of curvature equal to 20 nm. The resonant frequency typically was 270 kHz, and the measured (see description above) force constant was 40 N/m. The feed-back loop was locked to the amplitude of oscillation on the high-frequency side of the resonance peak. The control software allowed choice of offset forces in both modes, as well as scan speeds and time constants relevant to tracking the topography.

Results and discussion

Layer structure and calibration methods

Contact mode analysis will be considered first, since this is the most widely available SPM technique. The regularity of an ordered nanosphere layer is illustrated in the contact mode image in Fig. 1(a). Hexagonal packing is evident, as well as defect structures. A smaller field of view (Fig. 1b) was analysed by two-dimensional fast-Fourier transformation (2-D FFT) (Fig. 1c). From this it was shown that the average centre-to-centre spacing was 209 nm, in good agreement with the stated diameter of the spheres. It should be noted that the repeat spacing of a periodic structure will be independent of effects arising from the convolution of tip shape with surface topography. Single beads, of submicrometre dimensions, on the other hand, will produce images which cannot readily be deconvoluted, unless the shape of the actual tip is known. Single objects of known shape, or clusters of such objects without long-range order, therefore will not be suitable as size standards for lateral calibration. Additionally, a regular structure with a known repetition

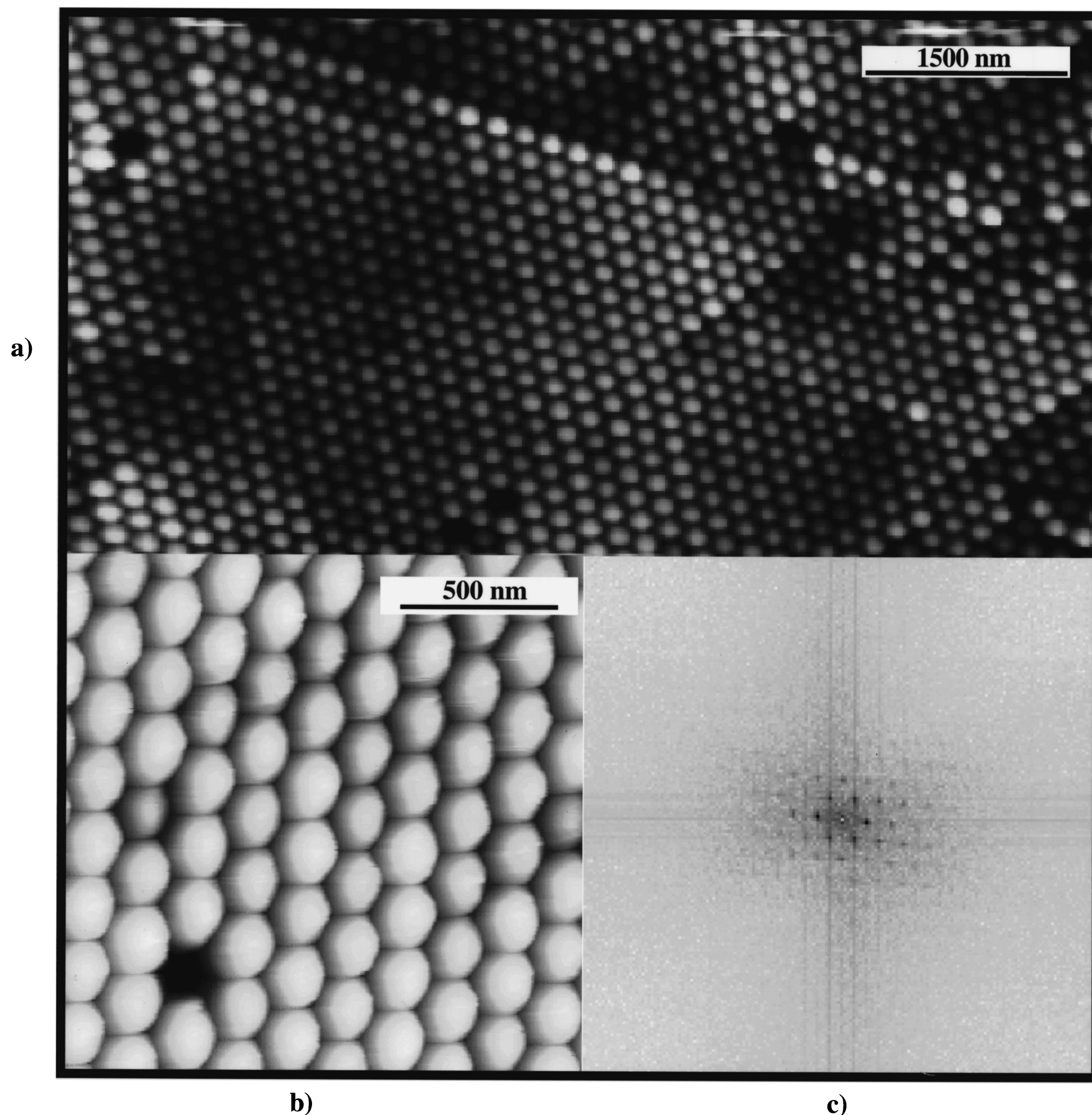

Fig. 1. Contact mode images of close-packed layers of 200-nm-diameter polystyrene beads, showing a large field of view (a) with long-range order and defect structures, and a smaller field of view (b). The results of applying the 2-D FFT method to the image in (b) are shown in (c); the spacings correspond to reciprocal lattice vectors of the hexagonal structure.

distance will allow determination of linearity and orthogonality, with the proviso that thermal drift must be allowed for.

Details of the resolved topography of the layers are shown in Fig. 2(a); the effects of tip shape are evident from the line profile along a close-packed direction (Fig. 2b). Simple geometrical considerations show that, in the contact mode, the ingress along the *z*-axis of a pyramidal tip with an aspect ratio of 0·7, and terminated by a spherical surface with a radius of curvature of 40 nm, along a close-packed direction through the centres of the beads, will be limited to some 45 nm. This is in good agreement with present results. However, this distance will be strongly dependent on the tip shape; it is therefore not a reliable distance for the purpose of vertical calibration. Likewise, it is not a useful measure of

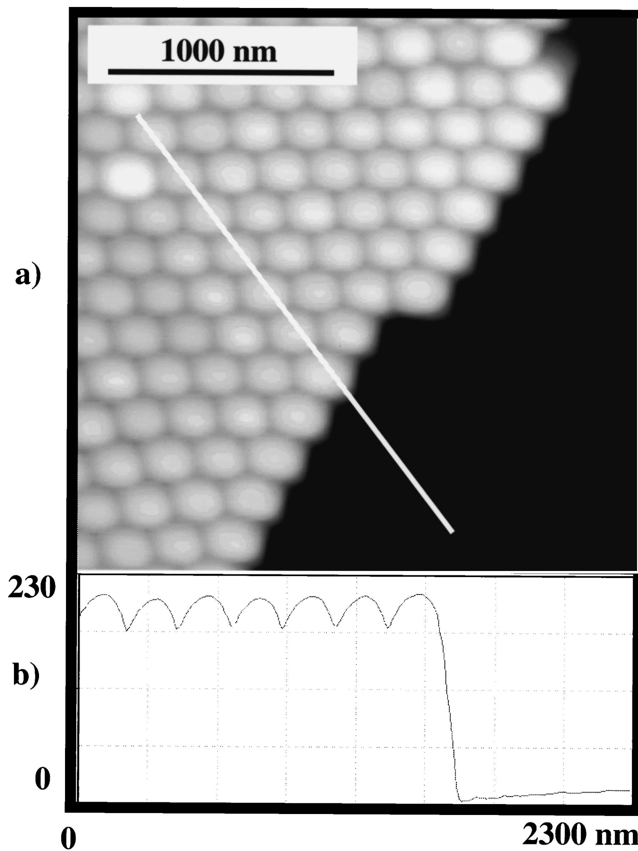

Fig. 2. (a) Contact mode image of a polystyrene bead layer at an edge. (b) A *z*-direction line profile along a close-packed axis, and extending to the edge, shows that the scanning stage is calibrated accurately along the *x*- and *y*-directions, and the step height provides calibration in the *z*-direction.

actual tip shape since the corrugation amplitude will depend on both the aspect ratio and the radius of curvature of the tip, as well as the direction of scanning as related to the orientation of the pyramid (the apex angle will depend on whether it defines a plane diagonal to the base corners, or one perpendicular to a base edge). The image of an edge of a close-packed layer, on the other hand, will have a step height, from the atomically flat substrate to the top of the layer, which is independent of the effects of convolution. The line profile in Fig. 2(b) illustrates this point. Close-packed ABAB ... multilayer structures occurred frequently, and exhibited multiple steps; these can provide the means for checking the *z*-calibration over a greater dynamic range. Alternatively, beads with larger, or smaller, diameters may be used.

Similar methodologies may be used in the noncontact mode. A typical noncontact mode image of a hexagonally close-packed layer of 200-nm beads is shown in Fig. 3(a). Image analysis with the line profile method (Fig. 3b) results in good lateral calibration. Alternatively, the 2-D FFT method will lead to a similar outcome (217 nm in this case), but with additional information concerning orthogonality and linearity. Again, attention must be given to the effects of thermal drift. Finally, calibration of the *z*-direction can be effected from images of edges of monolayers, as shown in Fig. 4(a, b). The results of applying the various calibration methods are summarized in Table 2.

Image artefacts

Artefacts arise in SPM due to various circumstances, and for various reasons. More specifically, AFM artefacts arise principally because of convolution between tip shape and surface topography (e.g. Thundat *et al.*, 1992; Odin *et al.*, 1994; Schwartz *et al.*, 1994). In STM, on the other hand, 'minitips' are the source of the most common and prominent artefacts; these occur when the tunnel current is momentarily delocalized. However, shape convolution effects also occur in STM, and affect the image quality for highly corrugated surfaces (Mantovani *et al.*, 1990; Barbet *et al.*, 1993). Conversely, delocalization of the interatomic interaction, whether repulsive or attractive, is not generally

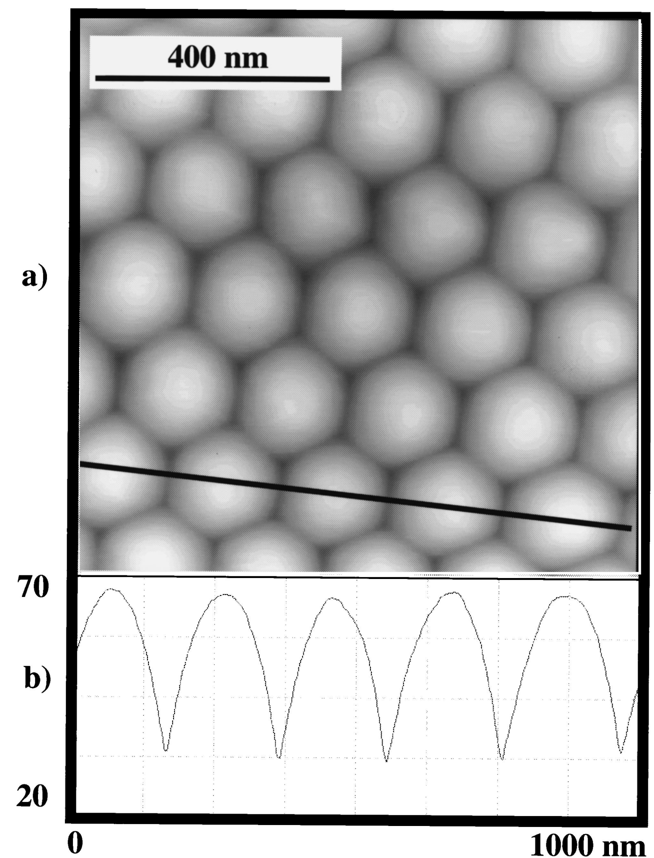

Fig. 3. (a) Noncontact mode image of a close-packed layer of 200-nm polystyrene beads. (b) Line profile along a close-packed axis. Analysis by the 2-D FFT method was also carried out; the results are not shown, in the interest of brevity.

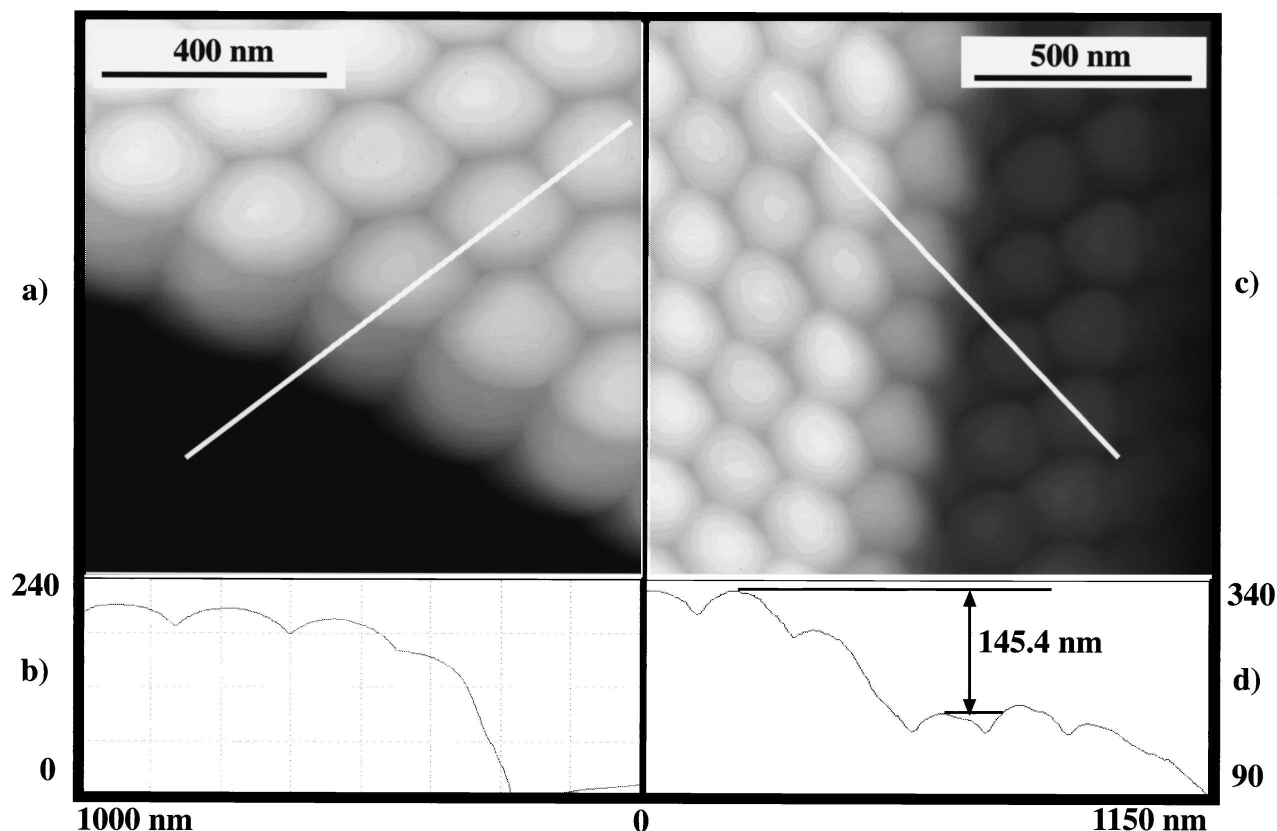

Fig. 4. (a, b) Demonstration of the line profile method for calibrating *z*-scan direction at the edge of a layer of beads, in the noncontact mode. The image in (c) and line profile in (d) show step of height equivalent to the *c*-spacing for an ideal close-packed structure. The line profiles (b) and (d) both demonstrate artefactual 'ghosts' at the edges of layers.

considered to be a significant cause of image artefacts in AFM. During the course of exploring noncontact imaging we observed artefactual effects that appeared as a consequence of both shape convolution and force delocalization. (We define 'delocalization' in the present context as describing a gradual, or sudden, change in the dimension and shape of the spatial extent, and/or a location-dependent strength, of the interaction between tip and surface.)

Anomalies were observed at edges of monolayers (Fig. 4a, b) and at steps of multilayer structures (Fig. 4c, d). The line profiles show that at steps there are 'ghosts' with dimensions which are not consistent with those of the actual 200-nm beads (and it should be noted that the ghosts were absent in contact mode scanning over similar fields of view). The layer spacing of 145 nm in Fig. 4(d) was in good agreement with the expected result for an ideal close-packed structure, however.

Table 2. Summary of outcomes of AFM calibration methods.

Figure	Spacing* (nm)	*z*-Height* (nm)	Method	Mode	Scanner (μm)
1(b,c)	209	–	2-D FFT	Contact	10
2(a,b)	217	210	Linescan	Contact	10
3(a,b)	202	–	Linescan	Noncontact	1
†	217	–	2-D FFT	Noncontact	10
4(b)	—	208	Linescan	Noncontact	10

*A statistical analysis of the full data base resulted in uncertainties of $\pm$6 nm (i.e. 3%) and $\pm$10 nm (i.e. 5%) for calibration in the *x*-*y* plane and along the *z*-axis, respectively. †This result was obtained from analysis of a similar field of view to that shown in Fig. 3(a).

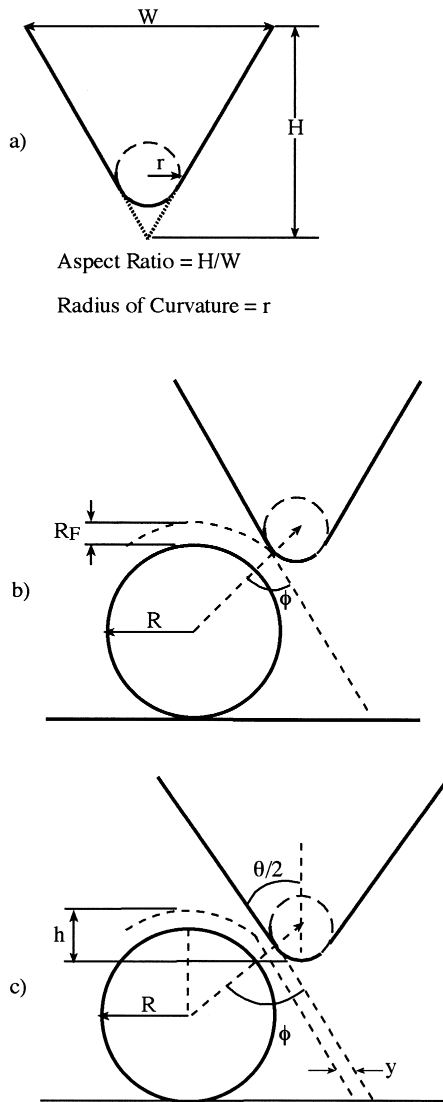

Fig. 5. (a) Schematic representation of the shape of an AFM tip. (b) Image generation from convolution of tip shape with the geometry of a spherical object, disregarding the effect of delocalization. (c) Image generation due to the combined effects of geometry of the tip–object system and force delocalization.

An AFM tip may be described as being a pyramid, with a given aspect ratio, terminated at the apex of a sphere of radius r, as illustrated in Fig. 5(a). The result of shape convolution between the tip and a spherical object, but disregarding force delocalization, is shown schematically in Fig. 5(b). The image will reproduce the shape of the sphere of radius R, albeit with a magnification due to the finite range, R_F, of the interaction, until the angle between the centre-to-centre line and the pyramidal face is $\phi = 90^\circ$. Below this point along the z-direction as related to the plane of the substrate the geometrical shadow of the tip shape will take over. The effect of delocalization is illustrated in Fig. 5(c). For angles $\phi < 90^\circ$ the interaction remains constant, and is defined by a columnar volume centred on the sphere-to-sphere line of direction. For $\phi \geq 90^\circ$ there will be a change due to the 'interaction volume' being defined by a sphere-to-plane interaction. (We use 'interaction volume' as a means of describing both the range and the lateral extent of the interaction.) In order to maintain a constant force the tip has to move away from the sphere of radius R, so as to increase the distance over which the interaction acts. Thus the 'ghost' should appear at the point when the centre-to-centre line is defined by $\phi \approx 90^\circ$. Simple geometry then shows that the anomaly will occur, in relation to the top of the sphere, at approximately

$$h = (R + r + R_F)[1 - \sin(\theta/2)] \qquad (1)$$

where $\sin(\theta/2) = W/2(H^2 + W^2/4)^{1/2}$; the symbols are defined in Fig. 5. Also, the width of the anomaly, y, will be approximately equal to the radius of curvature of the tip; the estimate represents the lateral travel required between the two limits of localization – sphere-to-sphere as related to sphere-to-plane. Viewed from the top, the 'ghost' will generate a concentric bulge around the sphere with an approximate inner radius, R', of

$$R' = (R + r + R_F)\cos(\theta/2). \qquad (2)$$

These effects will be negligible in the case of contact mode imaging, because of the short range (< 1 nm) of the interaction. However, in the noncontact case the ranges of candidate interactions are much longer. There is agreement between this qualitative description, and the images and line scans in Fig. 4. Detailed modelling is currently underway; the results suggest that simple Van der Waals interaction cannot account for the ghost features in the noncontact mode. However, meniscus forces do appear to explain the anomalies. A full account will be published.

A similar, although somewhat more complicated, artefact is illustrated in Fig. 6. In the centre of the image there is a vacant site, which gives the appearance of being occupied by a smaller sphere recessed below the top plane of the close-packed layer. This artefact is almost entirely a consequence of delocalization. When the tip is situated in the centre of the vacancy, the interaction volume is essentially an annular volume bridging the gap between the spherical section tip and the ring of six nearest neighbour beads The tip must therefore retract in order for a constant force to be maintained. When the tip moves off-centre in the vacancy, the interaction volume is reduced sharply to that linking one, or at most two, nearest neighbour beads. Accordingly the tip may now relax deeper into the vacancy.

Determination of tip parameters

The aspect ratio, H/W as defined in Fig. 5, of the tip and the radius of curvature, r, of the apex are the two principal parameters which determine the 'quality' of a tip. The aspect

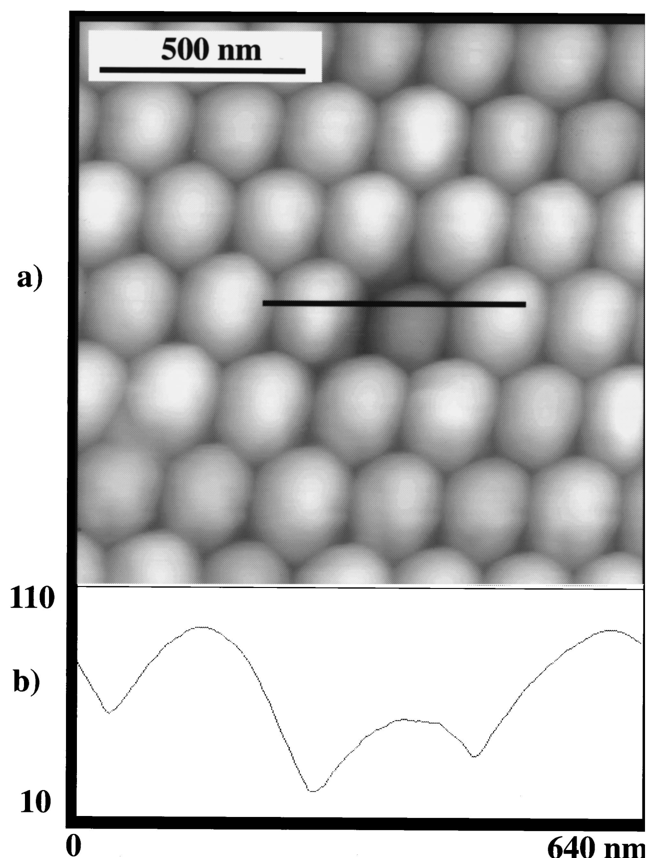

Fig. 6. Image (a) and line profile (b) for an artefact at a vacancy in a close-packed hexagonal monolayer of polystyrene beads – associated with the image formation process in the noncontact mode. The 'ghost' is due mainly to the effects of delocalization.

ratio can be determined by the simple expediency of measuring the angle of a contour line which represents the geometrical convolution of surface topography and tip shape. For instance, the contour line at the intersection with the substrate in Fig. 4(b) defines an angle of $\theta/2 = \tan^{-1}(W/2H)$. This is half the apex angle of the tip; in the present case using data from the scan in Fig. 4(a), we find an actual, as opposed to nominal, aspect ratio of $(2{\cdot}0 \pm 0{\cdot}5)$:1, which is in tolerable agreement with the nominal value of 3:1.

The actual radius of curvature for a particular tip can be determined, reliably and conveniently, from the 'ghost' feature in a noncontact mode image. The shoulder (Fig. 4b or d) occurs at a point of transition from sphere-to-sphere to sphere-to-plane interaction. The diagram in Fig. 5(c) shows that at this point

$$r = -(R + R_F) + R'/\cos(\theta/2). \quad (3)$$

Again, using results from the scan in Fig. 4, we find an actual value of $r = 25 \pm 15$ nm, for a particular tip, which brackets the nominal stated value of 20 nm. This method of determination is sufficiently convenient to permit frequent evaluation of tip quality before, during and after an experiment. The principal merit of this method, i.e. inferring r from features of the image of a perfect layer, is that it separates out the parameter for the aspect ratio from that of the radius of curvature.

Conclusions

These investigations have shown that 2-D structures of polystyrene beads in the size range from 100 nm and upwards can be tailored to explorations of the force microscopy system – consisting of tip, surface and interaction. The long-range order of the bead structures provides the means for lateral calibration, while the layer spacing constitutes a reliable and adjustable measure of height along the z-axis.

It is well known that AFM as a tool for visualization in the submicrometre range is currently limited by artefacts due to convolution of tip shape with surface topography. It is not generally appreciated, however, that delocalization of the tip-to-surface interaction is the cause of other artefacts. The polystyrene bead structures lend themselves to investigations of both classes of artefacts, as demonstrated above.

At a more fundamental level – having complete knowledge of both tip and surface – it is possible, in principle, to probe the interactions, and thus shed light on current theories of interactions which are operative in noncontact modes.

The ability of the AFM to monitor processes at surfaces and interfaces, *in situ* and in real time and space, is an attribute of particular significance for probing biological systems. It is noteworthy that polystyrene beads have numerous applications as biological substrates and as bioselective surfaces. Accordingly, it should be possible to design experiments which exploit the synergisms between AFM, polystyrene beads and biosystems.

Acknowledgments

This project was funded in part by the Australian Research Council and by Griffith University. Several conversations with Bradley Dinte were most successful.

References

Barbet, J., Garvin, A., Thimonier, J., Chauvin, J.-P. & Rocca-Serra, J. (1993) Scanning tunneling microscopy of colloidal gold particles. *Ultramicroscopy*, **50**, 355–363.

Binnig, G., Quate, C.F. & Gerber, C. (1986) Atomic force microscope. *Phys. Rev. Lett.* **56**, 930–933.

Binnig, G., Röhrer, H., Gerber, C. & Weibel, E. (1982) Surface studies by scanning tunneling microscopy. *Phys. Rev. Lett.* **49**, 57–61.

Li, Y. & Lindsay, S.M. (1991) Polystyrene latex particles as a size calibration for the atomic force microscope. *Rev. Sci. Instrum.* **62**, 2630–2633.

Mantovani, J.G., Allison, D.P., Warmack, R.J., Ferrell, T.L., Ford, J.R., Manos, R.E., Thompson, J.R., Reddick, B.B. & Jacobson, K.B. (1989) Scanning tunnelling microscopy of tobacco mosaic virus on evaporated and sputter-coated palladium/gold substrates. *J. Microsc.* **158,** 109–116.

Odin, C., Aime, J.P., El Kaakour, Z. & Bouhacina, T. (1994) Tip's finite size effects on atomic force microscopy in the contact mode: simple geometrical considerations for rapid estimation of apex radius and tip angle based on the study of polystyrene latex balls. *Surf. Sci.* **317,** 321–340.

Schwartz, U.D., Haefke, H., Reimann, P. & Güntherodt, H.-J. (1994) Tip artefacts in scanning force microscopy. *J. Microsc.* **173,** 183–197.

Thundat, T., Zheng, X.-Y., Sharp, S.L., Allison, D.P., Warmack, R.J., Joy, D.C. & Ferrell, T.L. (1992) Calibration of atomic force microscope tips using biomolecules. *Scanning Microsc.* **6,** 903–910.

Wickramasinghe, H.K. (1990) Scanning probe microscopy: current status and future trends. *J. Vac. Sci. Technol. A,* **8,** 363–368.

Wurster, R. & Ocker, B. (1993) Investigation of nanoparticles by atomic and lateral force microscopy. *Scanning,* **15,** 130–135.

Xu, S. & Arnsdorf, M.F. (1994) Calibration of the scanning (atomic) force microscope with gold particles. *J. Microsc.* **173,** 199–210.

Young, R.D., Ward, J. & Scire, F. (1972) The Topographiner: an instrument for measuring surface microtopography. *Rev. Sci. Instrum.* **43,** 999–1011.